Production of psi (2S) mesons in pp-bar collisions at 1.96 TeV

Citation: CDF Collaboration et al. "Production of psi (2S) mesons in pp-bar collisions at 1.96 TeV." Physical Review D 80.3 (2009): 031103. © 2009 The American Physical Society

As Published: http://dx.doi.org/10.1103/PhysRevD.80.031103

Publisher: American Physical Society

Persistent URL: http://hdl.handle.net/1721.1/51885

Version: Final published version: final published article, as it appeared in a journal, conference proceedings, or other formally published context

PHYSICAL REVIEW D **80,** 031103(R) (2009)

Production of $\psi(2S)$ mesons in $p\bar{p}$ collisions at 1.96 TeV

T. Aaltonen,[24] J. Adelman,[14] T. Akimoto,[56] B. Álvarez González,[12,u] S. Amerio,[44b,44a] D. Amidei,[35] A. Anastassov,[39] A. Annovi,[20] J. Antos,[15] G. Apollinari,[18] A. Apresyan,[49] T. Arisawa,[58] A. Artikov,[16] W. Ashmanskas,[18] A. Attal,[4] A. Aurisano,[54] F. Azfar,[43] W. Badgett,[18] A. Barbaro-Galtieri,[29] V. E. Barnes,[49] B. A. Barnett,[26] P. Barria,[47c,47a] V. Bartsch,[31] G. Bauer,[33] P.-H. Beauchemin,[34] F. Bedeschi,[47a] D. Beecher,[31] S. Behari,[26] G. Bellettini,[47b,47a] J. Bellinger,[60] D. Benjamin,[17] A. Beretvas,[18] J. Beringer,[29] A. Bhatti,[51] M. Binkley,[18] D. Bisello,[44b,44a] I. Bizjak,[31,z] R. E. Blair,[2] C. Blocker,[7] B. Blumenfeld,[26] A. Bocci,[17] A. Bodek,[50] V. Boisvert,[50] G. Bolla,[49] D. Bortoletto,[49] J. Boudreau,[48] A. Boveia,[11] B. Brau,[11,b] A. Bridgeman,[25] L. Brigliadori,[6b,a6a] C. Bromberg,[36] E. Brubaker,[14] J. Budagov,[16] H. S. Budd,[50] S. Budd,[25] S. Burke,[18] K. Burkett,[18] G. Busetto,[44b,44a] P. Bussey,[22] A. Buzatu,[34] K. L. Byrum,[2] S. Cabrera,[17,w] C. Calancha,[32] M. Campanelli,[36] M. Campbell,[35] F. Canelli,[14,18] A. Canepa,[46] B. Carls,[25] D. Carlsmith,[60] R. Carosi,[47a] S. Carrillo,[19,o] S. Carron,[34] B. Casal,[12] M. Casarsa,[18] A. Castro,[6b,a6a] P. Catastini,[47c,47a] D. Cauz,[55b,55a] V. Cavaliere,[47c,47a] M. Cavalli-Sforza,[4] A. Cerri,[29] L. Cerrito,[31,q] S. H. Chang,[62] Y. C. Chen,[1] M. Chertok,[8] G. Chiarelli,[47a] G. Chlachidze,[18] F. Chlebana,[18] K. Cho,[62] D. Chokheli,[16] J. P. Chou,[23] G. Choudalakis,[33] S. H. Chuang,[53] K. Chung,[13] W. H. Chung,[60] Y. S. Chung,[50] T. Chwalek,[27] C. I. Ciobanu,[1] M. A. Ciocci,[47c,47a] A. Clark,[21] D. Clark,[7] G. Compostella,[44a] M. E. Convery,[18] J. Conway,[8] M. Cordelli,[20] G. Cortiana,[44b,44a] C. A. Cox,[8] D. J. Cox,[8] F. Crescioli,[47b,47a] C. Cuenca Almenar,[8,w] J. Cuevas,[12,u] R. Culbertson,[18] J. C. Cully,[35] D. Dagenhart,[18] M. Datta,[18] T. Davies,[22] P. de Barbaro,[50] S. De Cecco,[52a] A. Deisher,[29] G. De Lorenzo,[4] M. Dell'Orso,[47b,47a] C. Deluca,[4] L. Demortier,[51] J. Deng,[17] M. Deninno,[a6a] P. F. Derwent,[18] A. Di Canto,[47b,47a] G. P. di Giovanni,[1] C. Dionisi,[52b,52a] B. Di Ruzza,[55b,55a] J. R. Dittmann,[5] M. D'Onofrio,[4] S. Donati,[47b,47a] P. Dong,[9] J. Donini,[44a] T. Dorigo,[44a] S. Dube,[53] J. Efron,[40] A. Elagin,[54] R. Erbacher,[8] D. Errede,[25] S. Errede,[25] R. Eusebi,[18] H. C. Fang,[29] S. Farrington,[43] W. T. Fedorko,[14] R. G. Feild,[61] M. Feindt,[27] J. P. Fernandez,[32] C. Ferrazza,[47d,47a] R. Field,[19] G. Flanagan,[49] R. Forrest,[8] M. J. Frank,[5] M. Franklin,[23] J. C. Freeman,[18] I. Furic,[19] M. Gallinaro,[52a] J. Galyardt,[13] F. Garberson,[11] J. E. Garcia,[21] A. F. Garfinkel,[49] P. Garosi,[47c,47a] K. Genser,[18] H. Gerberich,[25] D. Gerdes,[35] A. Gessler,[27] S. Giagu,[52b,52a] V. Giakoumopoulou,[3] P. Giannetti,[47a] K. Gibson,[48] J. L. Gimmell,[50] C. M. Ginsburg,[18] N. Giokaris,[3] M. Giordani,[55b,55a] P. Giromini,[20] M. Giunta,[47a] G. Giurgiu,[26] V. Glagolev,[16] D. Glenzinski,[18] M. Gold,[38] N. Goldschmidt,[19] A. Golossanov,[18] G. Gomez,[12] G. Gomez-Ceballos,[33] M. Goncharov,[33] O. González,[32] I. Gorelov,[38] A. T. Goshaw,[17] K. Goulianos,[51] A. Gresele,[44b,44a] S. Grinstein,[23] C. Grosso-Pilcher,[14] R. C. Group,[18] U. Grundler,[25] J. Guimaraes da Costa,[23] Z. Gunay-Unalan,[36] C. Haber,[29] K. Hahn,[33] S. R. Hahn,[18] E. Halkiadakis,[53] B.-Y. Han,[50] J. Y. Han,[50] F. Happacher,[20] K. Hara,[56] D. Hare,[53] M. Hare,[57] S. Harper,[43] R. F. Harr,[59] R. M. Harris,[18] M. Hartz,[48] K. Hatakeyama,[51] C. Hays,[43] M. Heck,[27] A. Heijboer,[46] J. Heinrich,[46] C. Henderson,[33] M. Herndon,[60] J. Heuser,[27] S. Hewamanage,[5] D. Hidas,[17] C. S. Hill,[11,d] D. Hirschbuehl,[27] A. Hocker,[18] S. Hou,[1] M. Houlden,[30] S.-C. Hsu,[29] B. T. Huffman,[43] R. E. Hughes,[40] U. Husemann,[61] M. Hussein,[36] J. Huston,[36] J. Incandela,[11] G. Introzzi,[47a] M. Iori,[52b,52a] A. Ivanov,[8] E. James,[18] D. Jang,[13] B. Jayatilaka,[17] E. J. Jeon,[62] M. K. Jha,[a6a] S. Jindariani,[18] W. Johnson,[8] M. Jones,[49] K. K. Joo,[62] S. Y. Jun,[13] J. E. Jung,[62] T. R. Junk,[18] T. Kamon,[54] D. Kar,[19] P. E. Karchin,[59] Y. Kato,[42,n] R. Kephart,[18] W. Ketchum,[14] J. Keung,[46] V. Khotilovich,[54] B. Kilminster,[18] D. H. Kim,[62] H. S. Kim,[62] H. W. Kim,[62] J. E. Kim,[62] M. J. Kim,[20] S. B. Kim,[62] S. H. Kim,[56] Y. K. Kim,[14] N. Kimura,[56] L. Kirsch,[7] S. Klimenko,[19] B. Knuteson,[33] B. R. Ko,[17] K. Kondo,[58] D. J. Kong,[62] J. Konigsberg,[19] A. Korytov,[19] A. V. Kotwal,[17] M. Kreps,[27] J. Kroll,[46] D. Krop,[14] N. Krumnack,[5] M. Kruse,[17] V. Krutelyov,[11] T. Kubo,[56] T. Kuhr,[27] N. P. Kulkarni,[59] M. Kurata,[56] S. Kwang,[14] A. T. Laasanen,[49] S. Lami,[47a] S. Lammel,[18] M. Lancaster,[31] R. L. Lander,[8] K. Lannon,[40,t] A. Lath,[53] G. Latino,[47c,47a] I. Lazzizzera,[44b,44a] T. LeCompte,[2] E. Lee,[54] H. S. Lee,[14] S. W. Lee,[54,v] S. Leone,[47a] J. D. Lewis,[18] C.-S. Lin,[29] J. Linacre,[43] M. Lindgren,[18] E. Lipeles,[46] A. Lister,[8] D. O. Litvintsev,[18] C. Liu,[48] T. Liu,[18] N. S. Lockyer,[46] A. Loginov,[61] M. Loreti,[44b,44a] L. Lovas,[15] D. Lucchesi,[44b,44a] C. Luci,[52b,52a] J. Lueck,[27] P. Lujan,[29] P. Lukens,[18] G. Lungu,[51] L. Lyons,[43] J. Lys,[29] R. Lysak,[15] D. MacQueen,[34] R. Madrak,[18] K. Maeshima,[18] K. Makhoul,[33] T. Maki,[24] P. Maksimovic,[26] S. Malde,[43] S. Malik,[31] G. Manca,[30,f] A. Manousakis-Katsikakis,[3] F. Margaroli,[49] C. Marino,[27] C. P. Marino,[25] A. Martin,[61] V. Martin,[22,l] M. Martínez,[4] R. Martínez-Ballarín,[32] T. Maruyama,[56] P. Mastrandrea,[52a] T. Masubuchi,[56] M. Mathis,[26] M. E. Mattson,[59] P. Mazzanti,[a6a] K. S. McFarland,[50] P. McIntyre,[54] R. McNulty,[30,k] A. Mehta,[30] P. Mehtala,[24] A. Menzione,[47a] P. Merkel,[49] C. Mesropian,[51] T. Miao,[18] N. Miladinovic,[7] R. Miller,[36] C. Mills,[23] M. Milnik,[27] A. Mitra,[1] G. Mitselmakher,[19] H. Miyake,[56] N. Moggi,[a6a] M. N. Mondragon,[18,o] C. S. Moon,[62] R. Moore,[18] M. J. Morello,[47a] J. Morlock,[27] P. Movilla Fernandez,[18] J. Mülmenstädt,[29] A. Mukherjee,[18] Th. Muller,[27] R. Mumford,[26] P. Murat,[18] M. Mussini,[6b,a6a] J. Nachtman,[18,p] Y. Nagai,[56] A. Nagano,[56] J. Naganoma,[56] K. Nakamura,[56] I. Nakano,[41] A. Napier,[57] V. Necula,[17] J. Nett,[60] C. Neu,[46,x] M. S. Neubauer,[25] S. Neubauer,[27]

J. Nielsen,[29,h] L. Nodulman,[2] M. Norman,[10] O. Norniella,[25] E. Nurse,[31] L. Oakes,[43] S. H. Oh,[17] Y. D. Oh,[62] I. Oksuzian,[19] T. Okusawa,[42] R. Orava,[24] K. Osterberg,[24] S. Pagan Griso,[44b,44a] E. Palencia,[18] V. Papadimitriou,[18] A. Papaikonomou,[27] A. A. Paramonov,[14] B. Parks,[40] S. Pashapour,[34] J. Patrick,[18] G. Pauletta,[55b,55a] M. Paulini,[13] C. Paus,[33] T. Peiffer,[27] D. E. Pellett,[8] A. Penzo,[55a] T. J. Phillips,[17] G. Piacentino,[47a] E. Pianori,[46] L. Pinera,[19] K. Pitts,[25] C. Plager,[9] L. Pondrom,[60] O. Poukhov,[16,a] N. Pounder,[43] F. Prakoshyn,[16] A. Pronko,[18] J. Proudfoot,[2] F. Ptohos,[18,j] E. Pueschel,[13] G. Punzi,[47b,47a] J. Pursley,[60] J. Rademacker,[43,d] A. Rahaman,[48] V. Ramakrishnan,[60] N. Ranjan,[49] I. Redondo,[32] P. Renton,[43] M. Renz,[27] M. Rescigno,[52a] S. Richter,[27] F. Rimondi,[6b,a6a] L. Ristori,[47a] A. Robson,[22] T. Rodrigo,[12] T. Rodriguez,[46] E. Rogers,[25] S. Rolli,[57] R. Roser,[18] M. Rossi,[55a] R. Rossin,[11] P. Roy,[34] A. Ruiz,[12] J. Russ,[13] V. Rusu,[18] B. Rutherford,[18] H. Saarikko,[24] A. Safonov,[54] W. K. Sakumoto,[50] O. Saltó,[4] L. Santi,[55b,55a] S. Sarkar,[52b,55a] L. Sartori,[47a] K. Sato,[18] A. Savoy-Navarro,[1] P. Schlabach,[18] A. Schmidt,[27] E. E. Schmidt,[18] M. A. Schmidt,[14] M. P. Schmidt,[61,a] M. Schmitt,[39] T. Schwarz,[8] L. Scodellaro,[12] A. Scribano,[47c,47a] F. Scuri,[47a] A. Sedov,[49] S. Seidel,[38] Y. Seiya,[42] A. Semenov,[16] L. Sexton-Kennedy,[18] F. Sforza,[47b,47a] A. Sfyrla,[25] S. Z. Shalhout,[59] T. Shears,[30] P. F. Shepard,[48] M. Shimojima,[56,s] S. Shiraishi,[14] M. Shochet,[14] Y. Shon,[60] I. Shreyber,[37] P. Sinervo,[34] A. Sisakyan,[16] A. J. Slaughter,[18] J. Slaunwhite,[40] K. Sliwa,[57] J. R. Smith,[8] F. D. Snider,[18] R. Snihur,[34] A. Soha,[8] S. Somalwar,[53] V. Sorin,[36] T. Spreitzer,[34] P. Squillacioti,[47c,47a] M. Stanitzki,[61] R. St. Denis,[22] B. Stelzer,[34] O. Stelzer-Chilton,[34] D. Stentz,[39] J. Strologas,[38] G. L. Strycker,[35] J. S. Suh,[62] A. Sukhanov,[19] I. Suslov,[16] T. Suzuki,[56] A. Taffard,[25,g] R. Takashima,[41] Y. Takeuchi,[56] R. Tanaka,[41] M. Tecchio,[35] P. K. Teng,[1] K. Terashi,[51] J. Thom,[18,i] A. S. Thompson,[22] G. A. Thompson,[25] E. Thomson,[46] P. Tipton,[61] P. Ttito-Guzmán,[32] S. Tkaczyk,[18] D. Toback,[54] S. Tokar,[15] K. Tollefson,[36] T. Tomura,[56] D. Tonelli,[18] S. Torre,[20] D. Torretta,[18] P. Totaro,[55b,55a] S. Tourneur,[1] M. Trovato,[47d,47a] S.-Y. Tsai,[1] Y. Tu,[46] N. Turini,[47c,47a] F. Ukegawa,[56] S. Vallecorsa,[21] N. van Remortel,[24,c] A. Varganov,[35] E. Vataga,[47d,47a] F. Vázquez,[19,o] G. Velev,[18] C. Vellidis,[3] M. Vidal,[32] R. Vidal,[18] I. Vila,[12] R. Vilar,[12] T. Vine,[31] M. Vogel,[38] I. Volobouev,[29,v] G. Volpi,[47b,47a] P. Wagner,[46] R. G. Wagner,[2] R. L. Wagner,[18] W. Wagner,[27,y] J. Wagner-Kuhr,[27] T. Wakisaka,[42] R. Wallny,[9] S. M. Wang,[1] A. Warburton,[34] D. Waters,[31] M. Weinberger,[54] J. Weinelt,[27] W. C. Wester III,[18] B. Whitehouse,[57] D. Whiteson,[46,g] A. B. Wicklund,[2] E. Wicklund,[18] S. Wilbur,[14] G. Williams,[34] H. H. Williams,[46] P. Wilson,[18] B. L. Winer,[40] P. Wittich,[18,i] S. Wolbers,[18] C. Wolfe,[14] T. Wright,[35] X. Wu,[21] F. Würthwein,[10] S. Xie,[33] A. Yagil,[10] K. Yamamoto,[42] J. Yamaoka,[17] U. K. Yang,[14,r] Y. C. Yang,[62] W. M. Yao,[29] G. P. Yeh,[18] K. Yi,[18,p] J. Yoh,[18] K. Yorita,[58] T. Yoshida,[42,m] G. B. Yu,[50] I. Yu,[62] S. S. Yu,[18] J. C. Yun,[18] L. Zanello,[52b,52a] A. Zanetti,[55a] X. Zhang,[25] Y. Zheng,[9,e] and S. Zucchelli[6b,a6a]

(CDF Collaboration)

[1]Institute of Physics, Academia Sinica, Taipei, Taiwan 11529, Republic of China
[2]Argonne National Laboratory, Argonne, Illinois 60439, USA
[3]University of Athens, 157 71 Athens, Greece
[4]Institut de Fisica d'Altes Energies, Universitat Autonoma de Barcelona, E-08193, Bellaterra (Barcelona), Spain
[5]Baylor University, Waco, Texas 76798, USA
[a6a]Istituto Nazionale di Fisica Nucleare Bologna, I-40127 Bologna, Italy
[6b]University of Bologna, I-40127 Bologna, Italy
[7]Brandeis University, Waltham, Massachusetts 02254, USA
[8]University of California, Davis, Davis, California 95616, USA
[9]University of California, Los Angeles, Los Angeles, California 90024, USA
[10]University of California, San Diego, La Jolla, California 92093, USA
[11]University of California, Santa Barbara, Santa Barbara, California 93106, USA
[12]Instituto de Fisica de Cantabria, CSIC-University of Cantabria, 39005 Santander, Spain
[13]Carnegie Mellon University, Pittsburgh, Pennsylvania 15213, USA
[14]Enrico Fermi Institute, University of Chicago, Chicago, Illinois 60637, USA
[15]Comenius University, 842 48 Bratislava, Slovakia;
Institute of Experimental Physics, 040 01 Kosice, Slovakia
[16]Joint Institute for Nuclear Research, RU-141980 Dubna, Russia
[17]Duke University, Durham, North Carolina 27708, USA
[18]Fermi National Accelerator Laboratory, Batavia, Illinois 60510, USA
[19]University of Florida, Gainesville, Florida 32611, USA
[20]Laboratori Nazionali di Frascati, Istituto Nazionale di Fisica Nucleare, I-00044 Frascati, Italy
[21]University of Geneva, CH-1211 Geneva 4, Switzerland
[22]Glasgow University, Glasgow G12 8QQ, United Kingdom
[23]Harvard University, Cambridge, Massachusetts 02138, USA

[24]*Division of High Energy Physics, Department of Physics, University of Helsinki and Helsinki Institute of Physics, FIN-00014, Helsinki, Finland*
[25]*University of Illinois, Urbana, Illinois 61801, USA*
[26]*The Johns Hopkins University, Baltimore, Maryland 21218, USA*
[27]*Institut für Experimentelle Kernphysik, Universität Karlsruhe, 76128 Karlsruhe, Germany*
[28]*Center for High Energy Physics: Kyungpook National University, Daegu 702-701, Korea; Seoul National University, Seoul 151-742, Korea; Sungkyunkwan University, Suwon 440-746, Korea; Korea Institute of Science and Technology Information, Daejeon, 305-806, Korea; Chonnam National University, Gwangju, 500-757, Korea; Chonbuk National University, Jeonju 561-756, Korea*
[29]*Ernest Orlando Lawrence Berkeley National Laboratory, Berkeley, California 94720, USA*
[30]*University of Liverpool, Liverpool L69 7ZE, United Kingdom*
[31]*University College London, London WC1E 6BT, United Kingdom*
[32]*Centro de Investigaciones Energeticas, Medioambientales y Tecnologicas, E-28040 Madrid, Spain*
[33]*Massachusetts Institute of Technology, Cambridge, Massachusetts 02139, USA*
[34]*Institute of Particle Physics: McGill University, Montréal, Québec, Canada H3A 2T8; Simon Fraser University, Burnaby, British Columbia, Canada V5A 1S6; University of Toronto, Toronto, Ontario, Canada M5S 1A7; and TRIUMF, Vancouver, British Columbia, Canada V6T 2A3*
[35]*University of Michigan, Ann Arbor, Michigan 48109, USA*
[36]*Michigan State University, East Lansing, Michigan 48824, USA*
[37]*Institution for Theoretical and Experimental Physics, ITEP, Moscow 117259, Russia*
[38]*University of New Mexico, Albuquerque, New Mexico 87131, USA*
[39]*Northwestern University, Evanston, Illinois 60208, USA*
[40]*The Ohio State University, Columbus, Ohio 43210, USA*
[41]*Okayama University, Okayama 700-8530, Japan*
[42]*Osaka City University, Osaka 588, Japan*
[43]*University of Oxford, Oxford OX1 3RH, United Kingdom*
[44a]*Istituto Nazionale di Fisica Nucleare, Sezione di Padova-Trento, I-35131 Padova, Italy*
[44b]*University of Padova, I-35131 Padova, Italy*
[1]*LPNHE, Universite Pierre et Marie Curie/IN2P3-CNRS, UMR7585, Paris, F-75252 France*
[46]*University of Pennsylvania, Philadelphia, Pennsylvania 19104, USA*
[47a]*Istituto Nazionale di Fisica Nucleare Pisa, I-56127 Pisa, Italy*
[47b]*University of Pisa, I-56127 Pisa, Italy*
[47c]*University of Siena, I-56127 Pisa, Italy*
[47d]*Scuola Normale Superiore, I-56127 Pisa, Italy*
[48]*University of Pittsburgh, Pittsburgh, Pennsylvania 15260, USA*
[49]*Purdue University, West Lafayette, Indiana 47907, USA*
[50]*University of Rochester, Rochester, New York 14627, USA*
[51]*The Rockefeller University, New York, New York 10021, USA*
[52a]*Istituto Nazionale di Fisica Nucleare, Sezione di Roma 1, I-00185 Roma, Italy*
[52b]*Sapienza Università di Roma, I-00185 Roma, Italy*
[53]*Rutgers University, Piscataway, New Jersey 08855, USA*
[54]*Texas A&M University, College Station, Texas 77843, USA*
[55a]*Istituto Nazionale di Fisica Nucleare Trieste/Udine, I-34100 Trieste, Italy*
[55b]*University of Trieste/Udine, I-33100 Udine, Italy*
[56]*University of Tsukuba, Tsukuba, Ibaraki 305, Japan*
[57]*Tufts University, Medford, Massachusetts 02155, USA*
[58]*Waseda University, Tokyo 169, Japan*
[59]*Wayne State University, Detroit, Michigan 48201, USA*
[60]*University of Wisconsin, Madison, Wisconsin 53706, USA*
[61]*Yale University, New Haven, Connecticut 06520, USA*
[62]*Center for High Energy Physics: Kyungpook National University, Daegu 702-701, Korea; Seoul National University, Seoul 151-742, Korea; Sungkyunkwan University, Suwon 440-746, Korea; Korea Institute of Science and Technology Information, Daejeon, 305-806, Korea; Chonnam National University, Gwangju, 500-757, Korea*
(Received 14 May 2009; published 6 August 2009)

We have measured the differential cross section for the inclusive production of $\psi(2S)$ mesons decaying to $\mu^+\mu^-$ that were produced in prompt or B-decay processes from $p\bar{p}$ collisions at 1.96 TeV. These measurements have been made using a data set from an integrated luminosity of 1.1 fb^{-1} collected by the CDF II detector at Fermilab. For events with transverse momentum $p_T(\psi(2S)) > 2$ GeV/c and rapidity $|y(\psi(2S))| < 0.6$ we measure the integrated inclusive cross section $\sigma(p\bar{p} \to \psi(2S)X) \cdot \mathrm{Br}(\psi(2S) \to \mu^+\mu^-)$ to be $3.29 \pm 0.04(\mathrm{stat}) \pm 0.32(\mathrm{syst})$ nb.

DOI: 10.1103/PhysRevD.80.031103 PACS numbers: 14.40.Gx, 13.85.Ni, 13.20.Gd

The mechanism for producing heavy vector mesons in $p\bar{p}$ collisions is not well understood. The experimental measurement of prompt J/ψ and $\psi(2S)$ production cross sections by CDF in Tevatron run I [1] showed that the measured cross sections were 1 to 2 orders of magnitude larger than expected from the leading order color-singlet models. Theoretical efforts to improve the calculations added color octet contributions that increased the predicted cross sections, e.g., in the nonrelativistic QCD (NRQCD) model [2]. Recently there have been other approaches that do not directly introduce a color octet amplitude; rather, they incorporate the effects of multiple gluon processes during the production process, e.g., the k_T-factorization formalism [3] and the gluon tower model [4].

The NRQCD model with parametrized production matrix elements adjusted to data can successfully account for the Tevatron prompt $\psi(2S)$ cross section measurements, but it makes an unequivocal prediction of increasing transverse polarization of vector mesons as their transverse momentum p_T from production increases [2]. A recent polarization measurement at CDF [5] contradicts the NRQCD model prediction.

Experimentally, the extraction of direct J/ψ production information is complicated by significant feed-down from decays of promptly produced higher-mass charmonium states (χ_c, $\psi(2S)$) to J/ψ mesons. This is not a problem for direct $\psi(2S)$ production because there are no reported charmonium states with significant hadronic production cross sections that decay to the $\psi(2S)$. Consequently the $\psi(2S)$ provides an ideal testing ground for studying charmonium hadroproduction mechanisms. In this paper we present a measurement of the p_T dependence of the $\psi(2S)$ production cross section over the $\psi(2S)$ transverse momentum range $2 < p_T(\psi(2S)) < 30$ GeV/c with rapidity $|y(\psi(2S))| < 0.6$. This measurement greatly increases the statistical power of the data in the perturbative regime ($m_T \gg \lambda_{\mathrm{QCD}}$), facilitating comparison with theory.

We use data taken using the CDF II detector at the Fermilab Tevatron at 1.96 TeV [6]. The integrated luminosity of the data sample is 1.1 fb^{-1}. The CDF II detector, described in detail elsewhere [7], includes a tracking system in a solenoidal 1.4 T magnetic field. Electromagnetic and hadronic calorimeters backed by muon detectors surround the tracker. The essential detector elements for this analysis are the silicon strip tracking detector (SVX II), the central drift chamber (COT), and the central muon system (CMU and CMP). The CMU is a four-layer planar drift chamber system outside the CDF magnet coil and calorimeter steel (5 interaction lengths). The CMP is another muon chamber system behind the CMU, shielded by an

[a]Deceased.
[b]Visitor from University of Massachusetts Amherst, Amherst, MA 01003, USA.
[c]Visitor from Universiteit Antwerpen, B-2610 Antwerp, Belgium.
[d]Visitor from University of Bristol, Bristol BS8 1TL, United Kingdom.
[e]Visitor from Chinese Academy of Sciences, Beijing 100864, China.
[f]Visitor from Istituto Nazionale di Fisica Nucleare, Sezione di Cagliari, 09042 Monserrato (Cagliari), Italy.
[g]Visitor from University of California Irvine, Irvine, CA 92697, USA.
[h]Visitor from University of California Santa Cruz, Santa Cruz, CA 95064, USA.
[i]Visitor from Cornell University, Ithaca, NY 14853, USA.
[j]Visitor from University of Cyprus, Nicosia CY-1678, Cyprus.
[k]Visitor from University College Dublin, Dublin 4, Ireland.
[l]Visitor from University of Edinburgh, Edinburgh EH9 3JZ, United Kingdom.
[m]Visitor from University of Fukui, Fukui City, Fukui Prefecture, Japan 910-0017.
[n]Visitor from Kinki University, Higashi-Osaka City, Japan 577-8502.
[o]Visitor from Universidad Iberoamericana, Mexico D.F., Mexico.
[p]Visitor from University of Iowa, Iowa City, IA 52242, USA.
[q]Visitor from Queen Mary, University of London, London, E1 4NS, England, U.K.
[r]Visitor from University of Manchester, Manchester M13 9PL, England, U.K.
[s]Visitor from Nagasaki Institute of Applied Science, Nagasaki, Japan.
[t]Visitor from University of Notre Dame, Notre Dame, IN 46556, USA.
[u]Visitor from University de Oviedo, E-33007 Oviedo, Spain.
[v]Visitor from Texas Tech University, Lubbock, TX 79609, USA.
[w]Visitor from IFIC (CSIC-Universitat de Valencia), 46071 Valencia, Spain.
[x]Visitor from University of Virginia, Charlottesville, VA 22904, USA.
[y]Visitor from Bergische Universität Wuppertal, 42097 Wuppertal, Germany.
[z]On leave from J. Stefan Institute, Ljubljana, Slovenia.

additional 0.6 m of iron in the flux return yoke. In this analysis, we use only information provided by the central sector of the detector, with pseudorapidity $|\eta| < 0.6$.

Muon candidates are identified by a first-level hardware-based trigger that reconstructs a charged track in four axial layers of the COT [8]. The trigger then projects the track into the CMU/CMP system and matches the projected trajectory to a collection of three or four hits in the CMU muon system within a search window around the extrapolated track [9]. The dimuon trigger requires two opposite-sign muon candidates each having $p_T > 1.5$ GeV/c.

The $\psi(2S) \to \mu^+\mu^-$ candidates were reconstructed from muon pairs. The $\psi(2S)$ events may originate from the primary interaction (prompt) or from decays of B hadrons (B decay). In off-line reconstruction, each muon had to have at least three hits in the $r - \phi$ strips of SVX II in order to guarantee good vertex information to separate prompt and B-decay candidates. The minimum muon p_T is 2 GeV/c. If the CMU candidate has matching hits in the CMP chambers [7], the track p_T requirement is raised to 3 GeV/c to account for the extra iron traversed.

The $\psi(2S)$ mass and proper time distributions are used in a joint unbinned maximum likelihood fit to extract the prompt and B-decay signals in bins of p_T for $\psi(2S)$ candidates. The mass component separates signal from background, while the proper time component separates prompt $\psi(2S)$ events from those produced by B decays. The mass signal probability distribution function is the sum of a Gaussian plus an asymmetric function (CBF) [10] given by

$$\text{CBF} = \begin{cases} A \cdot e^{-((M-m_0)^2/2\sigma^2)} & \frac{M-m_0}{\sigma} > -\beta, \\ A \cdot (\frac{n}{\beta})^n \frac{e^{-(\beta^2/2)}}{(\frac{M-m_0}{\sigma}+\frac{n}{\beta}-\beta)^n} & \frac{M-m_0}{\sigma} \leq -\beta, \end{cases}$$

where m_0 is a fit parameter for the invariant mass peak, M is the dimuon invariant mass of each event, A is the normalization constant, the asymmetry parameter η is the relative fraction of mass parton distribution function (PDF) due to the symmetric Gaussian term, and empirical parameters β and n describe the tails of the function:

$$P_s^{\text{mass}} = \frac{\eta}{\sqrt{2\pi\sigma^2}} e^{-(M-m_o)^2/2\sigma^2} + (1-\eta)\text{CBF}(n, \beta, \sigma).$$

CBF parameters β and n and the asymmetry parameter η are fixed by a fit to all data over the entire p_T range, using the p_T dependence of the width parameter σ as given by simulation and fixing the absolute width in the highest p_T bin from this global fit. The σ values are the same in the explicit Gaussian and in the CBF term. The results of the global fit fix η to 0.834, meaning that the signal mass PDF is dominated by a symmetric single Gaussian function. The background mass PDF term is linear in mass.

The proper decay length ct is used to identify prompt and B-decay contributions to the mass signal. Here $ct = L_{xy}/(p_T/M)$, where L_{xy} is the transverse decay length projected onto the $\psi(2S)$ momentum. The prompt component is described by a double Gaussian function centered at zero (P_p^{ct}). The long-lived component is an exponential (P_{long}^{ct}). Because the $\psi(2S)$ events from B decay come from $B_h \to \psi(2S)X$, they do not have a B-hadron lifetime distribution. We use the effective lifetime of the B-decay signal as a fit parameter. Because it is defined in the $\psi(2S)$ rest frame, it is the same in all p_T bins. Finally, the background in the ct distribution is described by the sum of a prompt double Gaussian (P_{pb}^{ct}) plus three exponentials, each convolved with a Gaussian resolution function: one symmetric about zero (P_{sym}^{ct}), one for positive ct only (P_+^{ct}), and one for negative ct only (P_-^{ct}). The likelihood function is

$$\begin{aligned} L = {} & f_s P_s^{\text{mass}}[f_p P_p^{ct} + (1-f_p)P_{\text{long}}^{ct}] \\ & + (1-f_s)P_{bkg}^{\text{mass}}[f_{\text{sym}}P_{\text{sym}}^{ct} + f_+P_+^{ct} + f_-P_-^{ct} \\ & + (1-f_{\text{sym}}-f_+-f_-)P_{pb}^{ct}]. \end{aligned} \quad (1)$$

The population fractions include f_s, the $\psi(2S)$ signal fraction from the total number of candidates in the fit, f_p, the fraction of prompt $\psi(2S)$, f_{sym}, the fraction of symmetric long-lived background, f_+, the fraction of positive-ct long-lived background, and f_-, the fraction of negative-ct long-lived background.

The fit parameters are the width of the overall Gaussian in P_s^{mass}, the parameters of the double Gaussians for the prompt signal and background ct density distributions, the lifetime of the overall long-lived signal, the five data fractions f_i from Eq. (1), and the parameters of the long-lived background functions in each p_T bin. The fit projections in mass and proper time for $5.5 < p_T < 6.0$ GeV/c are shown in Fig. 1. Projecting the likelihood fits onto the mass distribution in each p_T bin gives χ^2 probabilities in the range [0.4–100]%. The fitted yields in each p_T bin are summarized in Table I. Signal events are classified as prompt or long lived by the fit parameter f_p. For each $\psi(2S)$ p_T bin we know the total number of events N. The fit returns the signal fraction f_s and its uncertainty σ_{f_s}. The

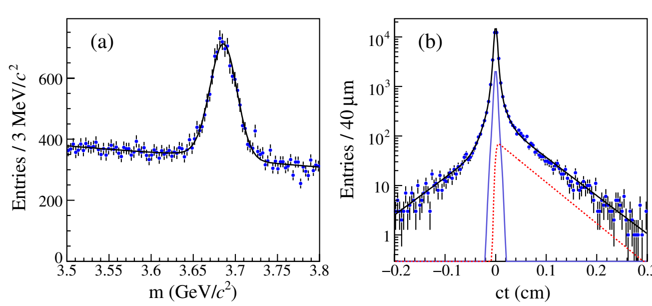

FIG. 1 (color online). The projections on the invariant mass (a) and the proper decay length (b) for $5.5 < p_T < 6.0$ GeV/c. The fitted curve for total signal plus background is overlaid on the data points. The prompt (solid lines) and long-lived (dashed lines) proper time signal curves are shown separately.

TABLE I. Event yields from the unbinned maximum likelihood fit and prompt event fraction. Transverse momenta are in GeV/c. The uncertainties are statistical only.

p_T	$\langle p_T \rangle$	Signal	Prompt	Prompt fraction	B decay
2.0–2.5	2.3	1961 ± 99	1701 ± 96	0.867 ± 0.019	260 ± 39
2.5–3.0	2.8	5025 ± 157	4241 ± 152	0.844 ± 0.011	785 ± 58
3.0–3.5	3.2	7003 ± 177	5955 ± 170	0.850 ± 0.009	1048 ± 64
3.5–4.0	3.8	6902 ± 171	5754 ± 166	0.834 ± 0.009	1148 ± 63
4.0–4.5	4.2	7060 ± 160	5778 ± 153	0.818 ± 0.008	1282 ± 60
4.5–5.0	4.7	6612 ± 147	5376 ± 141	0.813 ± 0.008	1236 ± 57
5.0–5.5	5.2	5519 ± 133	4462 ± 127	0.809 ± 0.009	1057 ± 52
5.5–6.0	5.7	5236 ± 121	4213 ± 114	0.805 ± 0.009	1023 ± 50
6.0–6.5	6.2	4663 ± 111	3636 ± 108	0.780 ± 0.011	1027 ± 51
6.5–7.0	6.7	3961 ± 99	3105 ± 94	0.784 ± 0.011	857 ± 45
7.0–7.5	7.2	3173 ± 87	2408 ± 81	0.759 ± 0.012	765 ± 41
7.5–8.0	7.7	2735 ± 78	2066 ± 73	0.756 ± 0.013	668 ± 37
8.0–8.5	8.2	2209 ± 69	1589 ± 62	0.720 ± 0.014	619 ± 35
8.5–9.0	8.7	1804 ± 62	1261 ± 56	0.699 ± 0.016	543 ± 32
9.0–9.5	9.2	1418 ± 55	987 ± 49	0.696 ± 0.019	430 ± 29
9.5–10.0	9.7	1170 ± 50	800 ± 45	0.684 ± 0.021	369 ± 27
10.0–11.0	10.5	1692 ± 60	1134 ± 54	0.670 ± 0.018	558 ± 33
11.0–12.0	11.5	1206 ± 51	810 ± 45	0.672 ± 0.021	395 ± 28
12.0–13.0	12.5	788 ± 41	511 ± 36	0.648 ± 0.026	277 ± 23
13.0–14.0	13.5	560 ± 35	331 ± 30	0.591 ± 0.032	229 ± 21
14.0–15.0	14.5	410 ± 29	240 ± 25	0.586 ± 0.036	170 ± 17
15.0–17.5	16.1	519 ± 36	284 ± 30	0.547 ± 0.036	235 ± 22
17.5–20.0	18.6	242 ± 26	129 ± 22	0.535 ± 0.058	112 ± 15
20.0–25.0	22.1	202 ± 25	117 ± 22	0.577 ± 0.063	86 ± 14
25.0–30.0	27.1	74 ± 17	45 ± 14	0.609 ± 0.106	29 ± 9

signal yield is $S = f_s \cdot N$; $\sigma_S^2 = (\sigma_{f_s} \cdot N)^2 + N \cdot f_s^2$. Analogous equations hold for the prompt yield $P = f_p \cdot S$ and the B-decay yield $B = (1 - f_s) \cdot S$. The correlation between the signal fraction and the prompt fraction is considered in the uncertainty of the prompt and B-decay yield. The number of prompt and B-decay events are also listed in Table I.

We have checked the p_T dependence of all the fit parameters. The variation is smooth and shows no indications of rapid changes of the background functions at any p_T. The prompt fraction decreases approximately linearly in the interval $2 < p_T < 30$ GeV/c.

The differential cross section is evaluated using the expression

$$\frac{d\sigma(\psi(2S))}{dp_T} = \frac{N(\psi(2S))}{\mathcal{A} \cdot \varepsilon_{\text{reco}} \cdot \int \mathcal{L} dt \cdot \Delta p_T}. \quad (2)$$

Here $\frac{d\sigma(\psi(2S))}{dp_T}$ is the average cross section for $\psi(2S)$ production in the given p_T bin integrated over rapidity in the range $|y| \leq 0.6$, $N(\psi(2S))$ is the number of $\psi(2S)$ events determined by the fit, $\mathcal{A}$ is the geometric acceptance combined with the CDF dimuon trigger efficiency, $\varepsilon_{\text{reco}}$ is the reconstruction efficiency, $\int \mathcal{L} dt$ is the integrated luminosity of the data set, and Δp_T is the width of the p_T bin. The acceptance and reconstruction efficiency are determined as follows.

The geometric acceptance is calculated by a Monte Carlo simulation (MC) method, using $\psi(2S) \to \mu^+\mu^-$ decays generated uniformly for $1 < p_T < 40$ GeV/c, $|y| < 1$, and $0 \leq \phi \leq 2\pi$. The $\psi(2S)$ decays are handled by EVTGEN [11], allowing us to specify the decay polarization as transverse, longitudinal, or unpolarized. We generate independent MC sets for these three options. Tracking proceeds from the large-radius detectors inward, and matching silicon hits are added to COT tracks. This makes the geometric acceptance insensitive to displacements of the $\psi(2S)$ decay point on the scale of 1 mm, typical of B-hadron flight paths in CDF. Therefore we use the same MC samples for calculating the geometric acceptance for both prompt and B-decay events. The systematic uncertainty for this assumption is negligible.

The MC events are passed through the CDF II GEANT-based simulation [12] and the standard CDF reconstruction. Events that pass the geometric selection are accepted based on each event's dimuon trigger efficiency, derived from CDF data for muon pairs having $|y| \leq 0.6$ with each muon having $p_T \geq 2$ GeV/c [13]. Variations with run and luminosity are included in the measurements. The prompt MC sample was analyzed with the likelihood fitter to check for p_T variations in prompt selection efficiency. None were seen.

Determining $\mathcal{A}$ is sensitive to the $\psi(2S)$ polarization parameter α, which defines the muon decay angular distribution in the vector meson rest frame: $dN/d\cos\theta = 1 + \alpha\cos^2\theta$. The polar angle θ is measured from the vector meson's direction in the laboratory frame.

We have previously measured the $\psi(2S)$ polarization in three p_T bins for prompt events and the average polarization in B-decay events [5]. With 15% probability a χ^2 fit shows that the three measured points are consistent with $\alpha = 0$. We use this as a basis to make the assumption that the polarization parameter α is constant over the p_T range of the data. Averaging the three measured points gives an average parameter $\alpha = 0.01 \pm 0.13$, which is used to determine $\mathcal{A}$ and its polarization-dependent systematic uncertainty. The prompt acceptance $\mathcal{A}$ varies from 2% at $p_T = 3$ GeV$/c$ to 20% at $p_T = 23$ GeV$/c$.

For B-decay events we use the same procedure. The polarization dependence is calculated using the measured B-decay polarization $\alpha_{\rm eff} = 0.36 \pm 0.25 \pm 0.03$ [5]. The B-decay acceptance varies from 1.5% at $p_T = 3$ GeV$/c$ to 19% at $p_T = 23$ GeV$/c$. Since the polarization is different for the prompt and B-decay events, a weighted average of the acceptances in each p_T bin is used for the inclusive differential cross section.

The reconstruction efficiency is the product of tracking and muon selection efficiencies measured in CDF data, including the tracking efficiencies for the COT (0.996 ± 0.009), SVX II (0.958 ± 0.006), and the dimuon tracking and selection efficiency (0.875 ± 0.019). Combining all the factors and adding the uncertainties in quadrature gives $\varepsilon_{\rm reco} = 0.805 \pm 0.038$.

Because the instantaneous CDF trigger rate might exceed our data handling capacity, the dimuon trigger, like many others, is prescaled. The integrated luminosity for the data sample has to be reduced by the luminosity-dependent dimuon trigger prescale factor to calculate the cross section. This is done on a run-by-run basis and has negligible statistical or systematic uncertainty. The 1.1 fb^{-1} sample luminosity is reduced to 0.95 fb^{-1} for this trigger. The resulting inclusive cross sections for prompt and B-decay production are listed in Table II. The prompt and B-decay data are plotted versus p_T in Fig. 2(a). Data from the run I CDF measurement [1] are also included in Fig. 2(b).

The major systematic uncertainties on these results are due to the systematic uncertainty in the luminosity determination (6%) [14] and the polarization uncertainty in the

TABLE II. The differential cross section (pb/GeV$/c$) times the dimuon branching fraction as a function of p_T for $|y| \leq 0.6$. For the B-decay measurement the symbol Br includes the branching fraction for b quark inclusive decay to $\psi(2S)X$ as well as the dimuon branching fraction of $\psi(2S)$.

p_T (GeV$/c$)	Inclusive $\frac{d\sigma}{dp_T}\cdot$ Br (pb/GeV$/c$)	Prompt $\frac{d\sigma}{dp_T}\cdot$ Br (pb/GeV$/c$)	B decay $\frac{d\sigma}{dp_T}\cdot$ Br (pb/GeV$/c$)
2.0–2.5	1144 ± 58 ± 132	953 ± 54 ± 113	191 ± 28 ± 45
2.5–3.0	1153 ± 36 ± 112	946 ± 34 ± 95	207 ± 15 ± 32
3.0–3.5	1037 ± 26 ± 102	856 ± 24 ± 87	181 ± 11 ± 30
3.5–4.0	779 ± 19 ± 73	630 ± 18 ± 61	149 ± 8 ± 23
4.0–4.5	611 ± 14 ± 60	483 ± 13 ± 49	128 ± 6 ± 21
4.5–5.0	490 ± 11 ± 48	383 ± 10 ± 39	107 ± 5 ± 18
5.0–5.5	316 ± 8 ± 29	248 ± 7 ± 23	68 ± 3 ± 10
5.5–6.0	262 ± 6 ± 24	204 ± 6 ± 19	58 ± 3 ± 8
6.0–6.5	189 ± 5 ± 17	143 ± 4 ± 13	46 ± 2 ± 6
6.5–7.0	146 ± 4 ± 13	111 ± 3 ± 10	35 ± 2 ± 5
7.0–7.5	105.4 ± 2.9 ± 9.5	77.1 ± 2.6 ± 7.1	28.3 ± 1.5 ± 3.8
7.5–8.0	81.9 ± 2.3 ± 7.4	59.8 ± 2.1 ± 5.5	22.1 ± 1.2 ± 2.9
8.0–8.5	60.9 ± 1.9 ± 5.5	42.1 ± 1.7 ± 3.9	18.8 ± 1.1 ± 2.5
8.5–9.0	45.4 ± 1.6 ± 4.0	30.5 ± 1.3 ± 2.7	14.9 ± 0.9 ± 1.8
9.0–9.5	32.3 ± 1.3 ± 2.8	21.8 ± 1.1 ± 1.9	10.5 ± 0.7 ± 1.2
9.5–10.0	25.9 ± 1.1 ± 2.2	17.2 ± 1.0 ± 1.5	8.7 ± 0.6 ± 0.9
10.0–11.0	17.7 ± 0.6 ± 1.5	11.4 ± 0.54 ± 1.0	6.3 ± 0.4 ± 0.7
11.0–12.0	11.96 ± 0.5 ± 1.1	7.72 ± 0.43 ± 0.69	4.24 ± 0.30 ± 0.51
12.0–13.0	7.33 ± 0.39 ± 0.64	4.56 ± 0.33 ± 0.40	2.77 ± 0.23 ± 0.31
13.0–14.0	5.03 ± 0.32 ± 0.44	2.85 ± 0.26 ± 0.24	2.18 ± 0.20 ± 0.24
14.0–15.0	3.42 ± 0.25 ± 0.29	1.93 ± 0.20 ± 0.16	1.49 ± 0.15 ± 0.15
15.0–17.5	1.61 ± 0.11 ± 0.14	0.85 ± 0.09 ± 0.07	0.76 ± 0.07 ± 0.08
17.5–20.0	0.68 ± 0.07 ± 0.06	0.35 ± 0.06 ± 0.03	0.33 ± 0.05 ± 0.03
20.0–25.0	0.27 ± 0.03 ± 0.02	0.15 ± 0.03 ± 0.01	0.12 ± 0.02 ± 0.01
25.0–30.0	0.089 ± 0.020 ± 0.007	0.053 ± 0.017 ± 0.004	0.036 ± 0.011 ± 0.003

acceptance calculation (9% at low p_T, 2% at high p_T). Other systematic uncertainties arise from p_T variations in the trigger ($< 3\%$) and reconstruction efficiencies (4.7%). Systematic uncertainties due to the mass shape parametrization, fitting function parametrization, and prompt fraction determination are all less than 1%. The data in Fig. 2 have both statistical and systematic uncertainties included.

The integrated cross sections are calculated by summing the differential cross sections across p_T bins. The systematic uncertainty on the integrated cross section is calculated by assuming that all sources of uncertainty are fully correlated among p_T bins, with the exception of the trigger efficiency uncertainty, which is uncorrelated among p_T bins. After calculating the uncertainty on the integrated cross section from each source, the total uncertainty is calculated by summing the individual contributions in quadrature.

The integrated inclusive differential cross section for $p_T > 2$ GeV$/c$ and $|y| < 0.6$ is measured to be

$$p_T(\psi(2S)) > 2\ \mathrm{GeV}/c \qquad \sigma(p\bar{p} \to \psi(2S)X) \cdot \mathrm{Br}(\psi(2S) \to \mu + \mu^-) = 3.29 \pm 0.04(\mathrm{stat}) \pm 0.32(\mathrm{syst})\ \mathrm{nb}.$$

For comparison to the run I measurement, we limit the p_T range to $p_T > 5$ GeV$/c$. Then the measured integrated inclusive cross section is

$$p_T(\psi(2S)) > 5\ \mathrm{GeV}/c \qquad \sigma(p\bar{p} \to \psi(2S)X) \cdot \mathrm{Br}(\psi(2S) \to \mu^+ \mu^-) = 0.69 \pm 0.01(\mathrm{stat}) \pm 0.06(\mathrm{syst})\ \mathrm{nb}.$$

At 1.8 TeV the integrated inclusive cross section for $p_T > 5$ GeV$/c$ and pseudorapidity <0.6 was $0.57 \pm 0.04^{+0.08}_{-0.09}$ nb [1]. The increase is $(21 \pm 19)\%$, compared to a theoretical prediction of $(14 \pm 8)\%$ based on changes in the parton energy distribution at the higher collision energy [15]. The uncertainty on the experimental ratio is dominated by the run I measurement due to its much lower statistics.

Prompt $\psi(2S)$ production has a harder p_T spectrum than that for J/ψ production [7]. We compute the ratio R of the two differential cross sections evaluated at the same p_T range for each vector meson. The p_T binning is matched to the J/ψ measurements of Ref. [7]. Since both measurements use the CDF apparatus, most systematic uncertainties cancel in the ratio. The luminosity uncertainty is fully correlated and is shown explicitly in the error bars in Fig. 3(a). The increase in the ratio at larger p_T reflects the slope difference. Even though it neglects any feed-down contributions to J/ψ prompt production, the model of Ref. [4] predicts the p_T dependence of this behavior, as shown by the dashed line in Fig. 3(a). The model prediction is normalized to these data in the p_T bin covering 8–9 GeV$/c$. This same behavior is seen in the ratio of cross sections for production from B decay, also shown in Fig. 3(a). The ratio of these two ratios is independent of p_T, as shown in Fig. 3(b). There is no theoretical motivation for this relation.

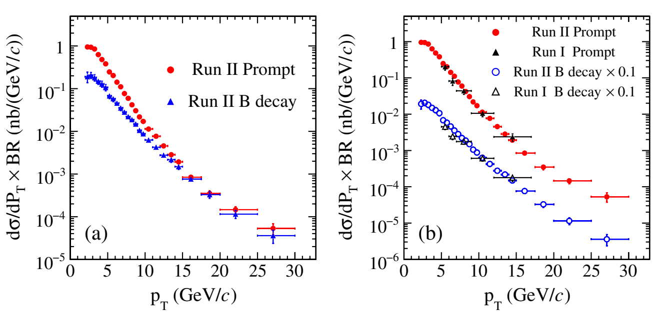

FIG. 2 (color online). (a) Prompt and B-decay production cross section distributions versus p_T for these data. (b) The same data with the run I points included. We ignore differences between rapidity and pseudorapidity for this comparison. The B-decay points have been scaled down by a factor of 10 for clarity of display.

In conclusion, we have measured the p_T dependence of the cross section for $\psi(2S)$ production in $p\bar{p}$ production at 1.96 TeV. These data have at least an order of magnitude more events than the run I measurements and show more precisely the trends seen in those data. The increase in the inclusive cross section at the higher energy of run II (1.96 TeV) compared to run I (1.8 TeV) agrees with expectations based on the increase in parton energy distribution.

These data extend the $\psi(2S)$ differential cross section measurement up to 30 GeV$/c$. They are an important input

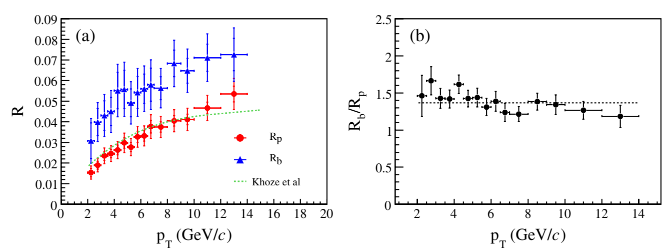

FIG. 3 (color online). (a) The differential cross section ratio of $\psi(2S)$ to J/ψ as a function of vector meson p_T for prompt events (R_p) and B-decay events (R_b). The main error bar on each point is the quadrature sum of the statistical and uncorrelated systematic uncertainties for that p_T bin. The extensions to the error bars show the correlated uncertainty from the luminosity. The dashed line is calculated using the prompt ratio predicted from Ref. [4] normalized to data for the p_T bin covering 8–9 GeV$/c$. (b) The ratio of B decay to prompt ratios R_b/R_p as a function of vector meson p_T. The fit to a constant gives a χ^2 of 13 for 14 degrees of freedom.

for an update of the matrix elements in the NRQCD factorization approach [2]. In the gluon tower model [4], the prompt hadroproduction of J/ψ, $\psi(2S)$, and Υ states has been calculated. The uncertainties of their calculation are rather large but their cross section prediction with adjusted parameters describes the published Tevatron data. In addition, their mechanism predicts a longitudinal polarization of J/ψ at large transverse momentum which agrees qualitatively with the recent Tevatron measurement [5]. We hope that in future calculations with this and other models the uncertainties can be reduced in order to make a meaningful comparison to these new cross section data. A successful description of both the cross section data and polarization measurements in the perturbative p_T region would demonstrate a good understanding of the charmonium hadroproduction mechanisms.

We thank the Fermilab staff and the technical staffs of the participating institutions for their vital contributions. This work was supported by the U.S. Department of Energy and the National Science Foundation; the Italian Istituto Nazionale di Fisica Nucleare; the Ministry of Education, Culture, Sports, Science and Technology of Japan; the Natural Sciences and Engineering Research Council of Canada; the National Science Council of the Republic of China; the Swiss National Science Foundation; the A. P. Sloan Foundation; the Bundesministerium für Bildung und Forschung, Germany; the Korean Science and Engineering Foundation and the Korean Research Foundation; the Science and Technology Facilities Council and the Royal Society, U.K.; the Institut National de Physique Nucleaire et Physique des Particules/CNRS; the Russian Foundation for Basic Research; the Ministerio de Ciencia e Innovación, and Programa Consolider-Ingenio 2010, Spain; the Slovak R&D Agency; and the Academy of Finland.

[1] F. Abe *et al.* (CDF Collaboration), Phys. Rev. Lett. **79**, 572 (1997).

[2] G. T. Bodwin, E. Braaten, and G. P. Lepage, Phys. Rev. D **51**, 1125 (1995); **55**, 5853(E) (1997); E. Braaten and S. Fleming, Phys. Rev. Lett. **74**, 3327 (1995). A discussion of recent developments in heavy quarkonium theory can be found in P. Artoisenet *et al.*, Phys. Rev. Lett. **101**, 152001 (2008). See also a recent review of this same work by J. P. Lansberg, Eur. Phys. J. C **61**, 693 (2009).

[3] S. P. Baranov, Phys. Rev. D **66**, 114003 (2002).

[4] V. A. Khoze, A. D. Martin, M. G. Ryskin, and W. J. Stirling, Eur. Phys. J. C **39**, 163 (2005).

[5] A. Abulencia *et al.* (CDF Collaboration), Phys. Rev. Lett. **99**, 132001 (2007).

[6] The CDF coordinate system has $\hat{z}$ along the proton direction, $\hat{x}$ horizontal pointing outward from the Tevatron ring, and $\hat{y}$ vertical. $\theta(\phi)$ is the polar (azimuthal) angle measured with respect to $\hat{z}$ and η is the pseudorapidity defined as $-\ln(\tan(\theta/2))$. The transverse momentum of a particle is denoted as $p_T = p\sin\theta$.

[7] D. Acosta *et al.* (CDF Collaboration), Phys. Rev. D **71**, 032001 (2005).

[8] E. J. Thomson *et al.*, IEEE Trans. Nucl. Sci. **49**, 1063 (2002).

[9] R. Downing *et al.*, Nucl. Instrum. Methods Phys. Res., Sect. A **570**, 36 (2007).

[10] J. Gaisser, Report No. SLAC-0255, 1982.

[11] D. J. Lange, Nucl. Instrum. Methods Phys. Res., Sect. A **462**, 152 (2001).

[12] E. Gerchtein and M. Paulini, arXiv:physics/0306031.

[13] D. Acosta *et al.* (CDF Collaboration), Phys. Rev. Lett. **93**, 032001 (2004).

[14] S. Klimenko, J. Konigsberg, and T. M. Liss, Report No. FERMILAB-N-741, 2003.

[15] K. Anikeev *et al.*, arXiv:hep-ph/0201071.